JOURNAL OF SPACECRAFT AND ROCKETS
Vol. 44, No. 2, March–April 2007

Comparison of Hydrogen and Hydrocarbon-Fueled Scramjet Engines for Orbital Insertion

M. R. Tetlow* and C. J. Doolan†
University of Adelaide, Adelaide, South Australia 5005, Australia

DOI: 10.2514/1.24739

This paper compares the performance of the scramjet-powered stages of two different launch systems: one using a hydrogen-fueled scramjet stage and one using a hydrocarbon-fueled scramjet stage. The two launch systems are optimized with respect to payload delivery capability and then compared, assuming a fixed launch mass. A rocket-powered booster is used to achieve the required scramjet ignition conditions, and a rocket-powered orbital stage is used to accelerate the payload from scramjet shutdown to low Earth orbit. The trajectory simulator includes a full spheroidal, rotating Earth model, a fourth-order gravitation model, and an MSISE93 atm model. A gradient projection optimization routine is used to achieve an optimal solution using a set of time-referenced vertical accelerations as optimization parameters. Hypersonic engine performance is determined using a quasi-one-dimensional scramjet model. Results show that a hydrogen-powered scramjet launch system outperforms a hydrocarbon-powered system, due to its higher specific impulse and peak Mach number. Although payload mass fractions are shown to be favorable, the high structural requirements of the scramjet imply that reusability is a key characteristic to make them financially viable. Trajectories were found to be dominated by their lift requirements, which outweighed any performance advantage for hydrocarbon fuels in terms of their better storage capability.

Nomenclature

A	=	area, m^2
a_{vert}	=	vertical component of acceleration, m^2/s
C_p	=	specific heat at constant pressure, J/kg/K
c	=	volumetric efficiency
c_f	=	skin friction coefficient
D	=	hydraulic diameter of scramjet combustor, m
d_F	=	injector port diameter/height, m
g	=	local gravitational acceleration, m^2/s
h	=	altitude, m, or enthalpy, J/kg
I_{sp}	=	specific impulse, s
L	=	lift, N
L_{inj}	=	injection location, m
L_{mix}	=	mixing length, m
M	=	Mach number
MW	=	molecular weight, kg/kmol
m	=	mass, kg
$\dot{m}$	=	mass flow rate, kg/s
P	=	atmospheric pressure, Pa
Pr	=	Prandtl number
p	=	pressure in scramjet combustor, Pa
Q_R	=	heating value of fuel, J/kg
R	=	universal gas constant, J/mol/K
T	=	temperature, K
t	=	time, s
U	=	gas velocity in scramjet, m/s
V	=	volume, m^3
V_∞	=	freestream velocity, m/s
$V_{\infty,\text{eff}}$	=	effective freestream velocity, m/s
x	=	distance along scramjet combustor, m
γ	=	ratio of specific heats
ε	=	fuel mass fraction
η_c	=	combustion efficiency
η_{KE}	=	kinetic energy efficiency
η_m	=	mixing efficiency
ρ	=	density, kg/m^3

Subscripts

aw	=	adiabatic wall
c	=	convective
cap	=	engine capture
comb	=	combustor
f	=	fuel
fuel	=	fuel mass
i	=	combustor inlet
noz	=	nozzle
ref	=	reference
sl	=	sea level
total	=	total mass
vac	=	vacuum
w	=	wall
0	=	local atmospheric, stagnation conditions, from injectors

I. Introduction

WITH the recent success of supersonic combustion ramjet (scramjet) atmospheric test flights [1,2], it is becoming increasingly likely that hypersonic air-breathing engines will be used for payload delivery to orbit. Scramjets have the advantage of burning atmospheric oxygen instead of an onboard oxidizer, as conventional rockets do. This not only reduces the size and mass of the vehicle but also increases the specific impulse by an order of magnitude [3]. These two factors make scramjets attractive to launch providers, because they have the potential to drive launch costs down. There are still many hurdles to overcome, such as control, aerodynamic heating, and combustion issues, but their use in future space launch systems is promising.

A number of fuel types have been investigated in the literature for use in scramjet propulsion systems, from solid [4] and liquid [5] hydrocarbon-based fuels to various phases of hydrogen [6]. Hydrocarbon fuels have a distinct advantage over hydrogen with respect to storage. Hydrocarbons have up to 11 times the storage density of hydrogen [7], making the tanks and, therefore, potentially the entire vehicle, much smaller compared with an equivalent

Received 20 April 2006; revision received 25 July 2006; accepted for publication 26 July 2006.

*Research Fellow, School of Mechanical Engineering. Member AIAA.
†Lecturer, School of Mechanical Engineering. Member AIAA.

propellant mass hydrogen-powered vehicle. Hydrogen does, however, have a significantly higher specific impulse [3,5]. In addition, hydrogen is the only fuel likely to deliver net positive levels of thrust at near-orbital velocities [7]. Hydrogen-fueled scramjets are believed to have an operating range of between Mach 5 and Mach 15 [3], with hydrocarbon-fueled scramjets expected to reach about Mach 10 [7] before thrust levels are reduced below useful values.

Either hydrogen or hydrocarbon fuels would be suitable for a powered scramjet flight segment; however, the mission profiles would be considerably different. Because of an operating limit of Mach 10 for hydrocarbon-fueled engines [7], the scramjet flight segment would be considerably shorter than that for a hydrogen-fueled vehicle. This would reduce the size of the scramjet stage, due to its shorter burn time, lower fuel mass requirement, and the fact that it has a higher fuel storage efficiency compared with a hydrogen-fueled scramjet. It would, however, also reduce the velocity increment contribution at the high specific impulse values that are possible using scramjet propulsion.

The limited operating range of scramjets means that another type of propulsion system is required, in addition to the scramjet, to achieve orbit from a stationary state. There are a number of possible solutions to this problem, including rocket and/or air-breathing systems or even a combination of the two, depending on the flight environment. Rocket propulsion systems have the advantage of being able to operate over all flight regimes encountered between a stationary state and orbit. Unfortunately, even the most efficient rocket engines are restricted to a specific impulse of around 430 s [8], making them considerably less efficient than air-breathing propulsion systems.

Turbojet and ramjet propulsion systems can achieve high specific impulse values, typically up to 7000 and 4000 s, respectively [3]; however, they are limited to velocities at or below that at which scramjets will ignite. This has led to a number of studies into combined cycle propulsion systems. Two of the best known examples of such combined cycle systems are the NASP [9] and SÄNGER [10] concept vehicles. These vehicles are much larger than those under investigation in this paper and rely not only on pure scramjet operation, but on complex systems capable of changing to suit many operating conditions (from turbojet through ramjet, scramjet, and, finally, to rocket mode) to achieve orbit. Although these systems may provide a better solution from a performance point of view, their complexity makes them less attractive in the near future. It was therefore decided to use a pure scramjet-powered stage in the present study, with conventional rockets providing propulsion before and after the scramjet stage.

Air-breathing scramjet engines require a certain minimum static pressure to maintain supersonic combustion. This is achieved by ensuring that the flight vehicle maintains a dynamic pressure above a minimum value of 9.5 kPa [9]. For the current study, the scramjet operating range was chosen to be well within the operating limits previously discussed, with ignition occurring at Mach 7 (92-KPa dynamic pressure) and shutdown occurring at Mach 15 (51-KPa dynamic pressure) and Mach 10 (58-KPa dynamic pressure) for the hydrogen and hydrocarbon-fueled vehicles, respectively. This equates to a dynamic pressure range between 175 and 50 kPa over the scramjet-powered flight phases. Scramjet ignition occurs at Mach 7, because successful flight tests have been demonstrated at this Mach number [1,2].

A number of different scramjet body configurations have been investigated in the literature in both ballistic [11] and waverider lifting body configurations [12]. Waveriders have high lift-to-drag ratios and therefore provide an efficient way of gaining energy from a lift force, at the expense of relatively little drag. Scramjet-powered waverider configuration vehicles have also been developed and tested [2] in previous studies. It was therefore decided to use a waverider lifting body configuration in the present study.

Another scramjet flight constraint is angle of attack. According to [9], the angle of attack of the scramjet intake should be limited to around 5 deg to maintain efficient scramjet performance. It should be noted that this limit defines an angle between the freestream velocity vector and the centerline of the inlet duct. The angle of interest from a trajectory modeling point of view is the angle between the freestream velocity and the lift force. To achieve a higher angle between the lift force and the freestream velocity, the lifting surfaces could be assumed to be at an angle relative to the centerline of the propulsion system. Because of the integrated design of a waverider, this variation is likely to be restrained to small values.

This paper consists of 10 parts. The first is this Introduction (Sec. I), which is followed by a brief survey of existing launch systems (Sec. II) to benchmark the work presented in this paper. Section III describes the launch vehicle system developed for this study. Section IV outlines the simulation and optimization procedure used and Sec. V details the quasi-one-dimensional scramjet combustor model used for the hypersonic propulsion segment of the flight. The mission profile is summarized (Sec. VI) before the calculated trajectory profiles are presented in Sec. VII. System mass and volume estimations (Sec. VIII) are compared for the hydrogen and hydrocarbon fuels before a discussion (Sec. IX) and conclusions (Sec. X).

II. Survey of Existing Launch Systems

To assess the performance of a new launch system, a comparison will need to be performed with existing launch systems. As launch systems vary considerably in start mass and payload delivery capability, the payload mass fraction will be used as a comparison measure. Large launch vehicles tend to have improved payload mass fractions, due to their improved propellant mass fractions [8]. Vehicles with similar payload capabilities will therefore be used for the comparison.

Table 1 shows that payload mass fractions for this class of launch vehicle are approximately 1% for a 200-km circular orbit. As expected, higher altitude orbits result in lower payload mass fractions. A 200-km circular orbit is used for comparison for the present study and a payload mass fraction of 0.9% (corresponding to the Long March CZ1D vehicle) will be the benchmark for comparison.

III. Vehicle Description

The launch system developed in this study consists of a two stage rocket-powered booster and a scramjet-powered waverider. The final rocket stage is housed in a payload bay inside the waverider. The total launch mass of the system is 9300 kg.

A. Booster Stages

The booster stages were required to achieve scramjet ignition conditions from a ground launch. A two stage booster was chosen, because this allows the correct altitude and flight path angle to be reached without spending a significant amount of time in the high-density lower altitudes. As the chosen altitude of 25 km at 0-deg flight path angle is relatively low, a single stage, nonrestartable booster would require a very shallow ascent trajectory to reach the required scramjet conditions. In addition, this type of trajectory would have a significantly higher integrated drag loss, due to its high velocity at low altitudes.

From the required propellant mass, the fully-fueled mass, without payload, was estimated using a structure mass fraction of 0.18. The first stage booster had a propellant mass of 2000 kg and the second stage booster a propellant mass of 4000 kg.

The propulsion system was modeled using an assumed propellant mass flow rate vs time profile. The specific impulse at specific

Table 1 Current launch vehicle performance [8]

Launch vehicle	Payload mass (mass fraction)	LEO altitude and inclination
ASLV	150 kg (0.36%)	400 km at 43 deg
M-3S11	780 kg (1.26%)	185 km at 31 deg
Long march CZ1D	720 kg (0.9%)	200 km at 28 deg
Start-1	360 kg (0.6%)	400 km at 90 deg

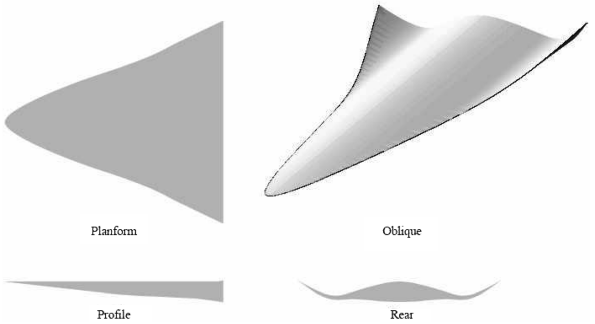

Fig. 1 Waverider vehicle [12].

altitudes was calculated using Eq. (1).

$$I_{sp} = I_{sp_{vac}} - \{[P(h)]/P_0\}(I_{sp_{vac}} - I_{sp_{sl}}) \tag{1}$$

where $P(h)$ is the local atmospheric pressure at the current altitude and P_0 is at sea level.

The aerodynamic coefficients for the boosters were calculated using a model developed for a conceptual launch vehicle called ArianeX [13]. The model provides lift and drag coefficients as a function of Mach number at zero angle of attack.

B. Scramjet (Waverider) Stage

Waveriders are hypersonic vehicles that ride the shock wave they produced during flight, thereby improving their lift-to-drag ratio [12]. An example of a waverider vehicle shape is shown in Fig. 1. Note that the model shown in Fig. 1 does not include a propulsion system. When the propulsion system is integrated into the waverider, Fig. 2 shows that the lift-to-drag ratio has a maximum value of around four [12].

The aerodynamic parameters for the waverider with an integrated scramjet propulsion system were taken from [6,12], providing drag and lift coefficients as a function of Mach number and angle of attack. Data were only available up to Mach 6, after which the aerodynamic data were extrapolated. The extrapolation involved linearly increasing the lift and drag coefficients by 10% between Mach 6 and Mach 16. This extrapolation was deemed satisfactory, due to the Mach number independence principle [14].

From the predetermined waverider start mass of 2000 kg and the average density for a hydrogen-fueled waverider, including payload, of 124 kg/m^3 [7], the volume of the vehicle could be estimated. From the required volume, Eq. (2) was used to approximate the aerodynamic reference area.

$$A_{ref} = cV^{\frac{2}{3}} \tag{2}$$

where c ranges between 0.2 and 0.8 for hypersonic cruise vehicles [7,15]. A value of 0.3 was used in this paper, because this represents a midrange value.

C. Orbital Stage

The orbital stage is a separate rocket stage that would be deployed from the scramjet payload bay and accelerate the payload from scramjet shutdown conditions to the required 200-km circular orbit. A structural mass fraction of 0.15 was used for the orbital stage with a specific impulse of 324 s. These values were taken from the upper stage of the Japanese H2 launch vehicle [8].

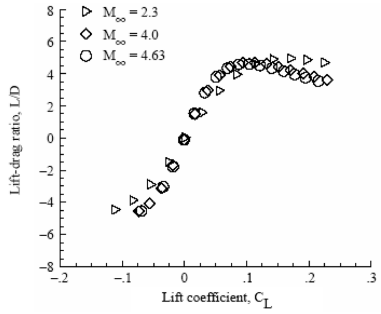

Fig. 2 Lift-to-drag ratio for a waverider with an integrated propulsion system [12].

IV. Simulation and Optimization

The software used was a FORTRAN-based code, originally developed at the Space Systems Institute in Stuttgart, Germany, and then modified for the purposes of this study. The dynamic equations were taken from [16] and describe a three-degree-of-freedom trajectory over a rotating Earth model, using a fourth-order Runge–Kutta integration technique. A spheroidal Earth model was used to determine the radius of the Earth at given latitudes. A fourth-order gravitational model [17] was implemented to approximate the Earth's gravitational field, and the atmospheric parameters were calculated using the mass spectrometer incoherent scatter 1993 (MSISE 93) atmosphere model [18].

A gradient projection optimization routing was used to optimize the trajectory, based on a minimum fuel consumption trajectory. The trajectory was parameterized using a set of six vertical accelerations as a function of time, which spanned the scramjet flight phase only. The final velocity of the scramjet-powered stage was used as a stopping condition for the integration, and the altitude and flight path angle were used as target constraints. The negative of the final mass was used as the optimization parameter. The lift force required was calculated using Eq. (3).

$$L = m[g - a_{vert}(t)] \tag{3}$$

where a_{vert} is a function of time. This acceleration profile produces the fuel minimum trajectory that achieves the correct target conditions.

Using Eq. (3), the required lift force can be determined. The waverider aerodynamic model is then used to determine the required angle of attack and the resulting drag force. The set of optimization parameters therefore define an angle-of-attack profile, which was restricted to between 0 and 6 deg.

V. Scramjet Propulsion Modeling

A. Quasi-One-Dimensional Model

A quasi-one-dimensional flow solver is used to model the flow properties within the scramjet combustor in order to calculate its overall thrust and specific impulse. Following the approach of [19], a series of ordinary differential equations (ODEs) were derived to describe the fluid motion within the scramjet duct. It is assumed that the supersonic flame is ignited and anchored by an additional device, thereby ensuring combustion is controlled by mixing rather than by chemical kinetics.

The equations solved are

$$\frac{dU}{dx} = \frac{1}{\alpha}\left[-\frac{1}{A}\frac{dA}{dx} + \left\{1 + \gamma M^2 - \frac{h_o}{h} + \frac{C_p T_f}{h}\right\}\frac{1}{\dot{m}}\frac{d\dot{m}}{dx} + \frac{1}{h}\left\{\frac{d\dot{m}}{dx}\frac{\eta_C Q_R}{\dot{m}}\right\} + 2\frac{c_f}{D}\left\{\gamma M^2 - \frac{C_p(T_{aw} - T_w)}{h\mathrm{Pr}^{2/3}}\right\}\right]$$

$$\frac{d\rho}{dx} = \rho\left[\frac{1}{\dot{m}}\frac{d\dot{m}}{dx} - \frac{1}{U}\frac{dU}{dx} - \frac{1}{A}\frac{dA}{dx}\right]$$

$$\frac{dp}{dx} = -\gamma p M^2\left[\frac{1}{U}\frac{dU}{dx} + \frac{1}{2}\left(\frac{4c_f}{D}\right) + \frac{1}{\dot{m}}\frac{d\dot{m}}{dx}\right]$$

$$\frac{dT}{dx} = T\left[\frac{1}{p}\frac{dp}{dx} - \frac{1}{\rho}\frac{d\rho}{dx}\right] \qquad \alpha = \frac{1}{U}\left[1 - \gamma M^2 + \frac{U^2}{h}\right] \qquad h = C_p T$$

$$C_p = \frac{\gamma R}{MW(\gamma - 1)} \tag{4}$$

The solver assumes ideal gas behavior and that a constant ratio of specific heats exists within the duct. Combustion takes the form of

releasing heat proportional to the mixing rate $\mathrm{d}\dot{m}/\mathrm{d}x$ multiplied by the heat of combustion. The heat of combustion is taken to be 116.7 MJ/kg for hydrogen fuel and 43.4 MJ/kg for jet A fuel.

The geometric area of the duct is numerically differentiated to yield the area derivative used in the system of equations (4), using a second-order accurate technique. Heat loss through the walls is related to the skin friction coefficient through the Reynold's analogy and is dependent on the adiabatic and actual wall temperatures. The skin friction coefficient is calculated using Eckert's reference method [14].

The Prandtl number is assumed constant and equal to 0.72. The pressure and temperature equations were derived using the differential forms of the conservation of mass and ideal gas equations. The specific heat is related to the gas constant and the molecular weight of the mixture. Thrust is calculated by integrating the pressure multiplied by the axial area increment along the combustor. Incorporated into this integration are the skin friction forces that act to retard scramjet motion.

The system of equations (4) is solved using the Lawrence Livermore ODEPACK system of solving stiff ODEs [20] using a computer code written in the FORTRAN programming language and integrated into the trajectory simulation software.

B. Supersonic Mixing Model

Typically, mixing of fuel and air is calculated by solving the Navier–Stokes equations in conjunction with a turbulence model. To keep the computational overhead low, the problem is simplified using the concept of mixing efficiency [Eq. (5)], which is defined as the ratio of fuel that is available for combustion to the amount that is released at the injector port.

$$\dot{m}_f = \eta_m \dot{m}_{f0} \tag{5}$$

where $\dot{m}_f$ is available for reaction. The mixing efficiency changes in value from zero at the injector exit to unity at a defined mixing length at which all the available fuel is mixed with the combustor air and is ready for combustion. A method for determining a suitable mixing length a priori can be found in [21]. However, for this study, the mixing length is set to the combustion chamber length. It is assumed that the scramjet fuel injection system will optimize the fuel–air mixing so that heat addition is spread over the available combustor length, in order to limit the occurrence of thermal choking.

An expression to describe the variation of mixing efficiency with combustion chamber length was found by using the multidimensional CFD results of Gerlinger and Brüggermann [22]. In their work, mixing efficiency was calculated along a hydrogen-fueled scramjet duct and compared with experimental measurements. These results show that mixing efficiency is reasonably independent of injector nozzle exit dimensions. Using the results from this study, the mixing efficiency was found to have the form

$$\eta_m = a(1 - e^{[-(k\bar{x})]^d}) \qquad a = 1.06492 \qquad k = 3.69639 \qquad d = 0.80586 \tag{6}$$

where $\bar{x} = (x - L_{\mathrm{inj}})/L_{\mathrm{mix}}$ and L_{inj} is the position along the duct at which injection begins. In this study, injection begins at the combustor entrance, hence, $L_{\mathrm{inj}} = 0$.

C. Propulsion Model Validation

To test the applicability of the models previously described, the experiments published in [23] were simulated using the quasi-one-dimensional solver. These experiments were performed in the T4 free-piston reflected shock tunnel at the University of Queensland. The shock tunnel operates by generating (via shock waves) a volume of high-temperature and high-pressure gas that supplies a hypersonic nozzle for a short period of time (~1–2 ms). In these tests, the shock tunnel was configured to produce a Mach 2.5 flow upstream of a scramjet duct, using a pair of wedges.

The scramjet combustor consisted of a fuel injector placed between two flat plates. The scramjet can be operated as either a constant area duct or as a diverging duct in which the top and bottom plates were set at equal angles of 1.72 deg. Table 2 summarizes the combustor inlet flow conditions published by [23] and used for the simulations. The subscript 0 represents stagnation conditions.

Table 2 Experimental duct entrance flow conditions [23]

Parameter	Value
T_0, K	2105
h_0, MJ/kg	2.4
p_0, kPa	1035
M_∞	2.47
p, kPa	59
T, K	1025
u, m/s	1560

Pressure was measured along the duct using an array of pressure transducers. Fuel was injected at the centerline of the duct through a slot $d_F = 1.6$-mm high to provide equivalence ratios ϕ between 0 and 1.05 in the constant area and diverging ducts.

For the constant area duct, it was found that boundary-layer separation occurred at an equivalence ratio of 0.29, and choking with subsonic combustion occurs at equivalence ratios higher than 0.43. Because flow separation represents a high energy loss condition in which scramjets should not be operated, a simulation was performed for a constant area duct experimental run with an equivalence ratio of 0.23. The pressure measurements along the duct are directly compared with the quasi-one-dimensional solver results in Fig. 3. Using the quoted experimental conditions, mixing layer properties were calculated to be $M_c = 0.16$, the fuel/air momentum ratio is 0.211, and $L_{\mathrm{mix}}/d_F = 195.75$ [21].

It can be seen that there is a good comparison between the simulation and mean experimental results. The simulation correctly models the mean pressure rise along the duct. It should be noted that the model correctly predicts the mixing length, because the exponential pressure rise ceases at the correct location.

Figure 4 shows a comparison between experimental results of [23] and the numerical model for a 1.72-deg diverging scramjet duct. Although not resolving reflected shock wave behavior, the code is able to reproduce the mean pressure distribution along the duct.

To account for the various loss mechanisms that occur within the combustor, such as incomplete combustion of the fuel and total pressure loss due to fuel/air mixing, a global combustion efficiency term is used that imposes an artificial limit on the amount of fuel that can be consumed. For comparison with the experimental results of [23], $\eta_c = 0.88$ gives good agreement. However, this value is only valid for an idealized combustor system that includes no flame holding, piloting, or mixing enhancement devices, all of which will increase the total pressure loss of the combustor flowfield and hence decrease the available thrust. For the trajectory modeling study presented in this paper, a conservative value of $\eta_c = 0.5$ is used in accordance with the scramjet propulsion estimates of [24].

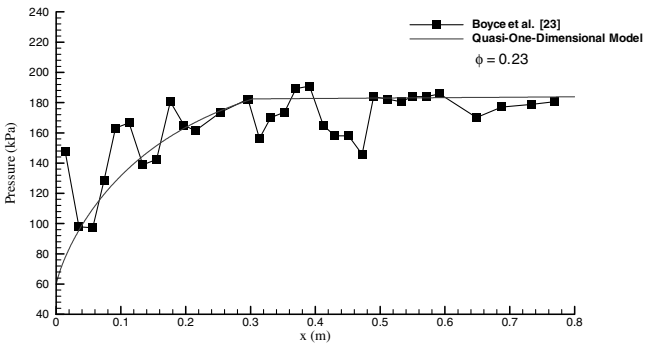

Fig. 3 Comparison between experimental constant area scramjet duct pressure measurements [23] and results simulated using the quasi-one-dimensional solver.

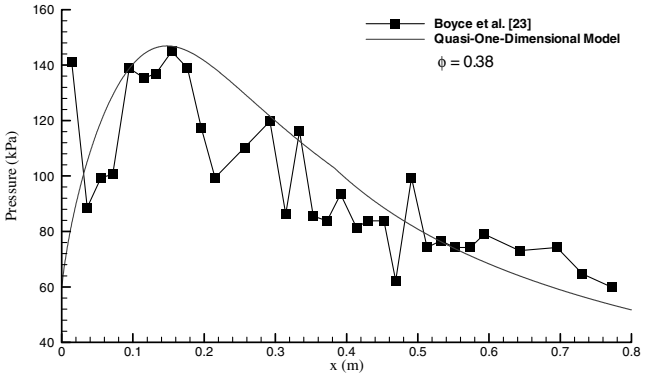

Fig. 4 Comparison between experimental diverging area scramjet duct pressure measurements [23] and results simulated using the quasi-one-dimensional solver.

D. Hypersonic Inlet Model

The combustor inlet conditions are calculated using an idealized hypersonic inlet model. The kinetic energy efficiency is used to reduce the freestream velocity to an effective value in order to compensate for total pressure loss in the inlet [Eq. (7)],

$$V_{\infty,\text{eff}} = \sqrt{\eta_{\text{KE}} V_{\infty}^2} \tag{7}$$

The kinetic energy efficiency is a function of the entropy rise across the inlet and is determined by the number of oblique shocks used to compress the incoming airstream. Heiser and Pratt [25] give a comprehensive analysis that compares the compression efficiency of single and multiple shock inlets. This analysis shows that a single oblique shock inlet has $\eta_{\text{KE}} = 0.93$ and a two-shock inlet has $\eta_{\text{KE}} = 0.96$, for a temperature ratio of 6. Further, Waltrup [26] presents a hypersonic inlet system that uses a combination of isentropic and oblique shock compression with $\eta_{\text{KE}} = 0.966$–0.974. For the trajectory analysis in this paper, a reasonable and conservative value of $\eta_{\text{KE}} = 0.96$ has been chosen. Increasing the kinetic energy efficiency to $\eta_{\text{KE}} = 0.974$ changes the specific impulse, as calculated by the scramjet model, by 2%.

To complete the inlet compression analysis, an effective freestream temperature and Mach number are calculated. Then the area ratio of the inlet is used in conjunction with the effective freestream conditions to calculate the combustor entrance conditions using a one-dimensional isentropic approach.

E. Scramjet Engine Dimensions for Trajectory Study

Figure 5 describes the scramjet engine dimensions used for the trajectory simulations. For all simulations, an inlet area capture ratio (A_{cap}/A_i) of 22 is assumed along with a capture area of 0.45 m^2. This results in a combustor inlet area of 0.02 m^2. As a means to illustrate the hypersonic inlet performance, the combustor inlet thermodynamic conditions ($x = 0$) at an altitude of 32 km and flight Mach number of 8 are calculated to be $M = 2.88$, $T = 1188.9$ K, and $p = 65.1$ kPa. These calculations were performed using the hypersonic inlet model described previously.

The combustor and nozzle lengths are each set to 1 m, making the overall engine 2-m long. For this study, the fuel–air mixing length is set to the combustor length. To evaluate the sensitivity of scramjet performance to uncertainties in mixing, it was found that a ±10% change in mixing length resulted in a ±0.01% change in scramjet specific impulse. The combustor area ratio (A_{comb}/A_i) is set to 11 and the nozzle area ratio ($A_{\text{noz}}/A_{\text{comb}}$) is set to 2.0. The equivalence ratio is set at 1.0 for all simulations.

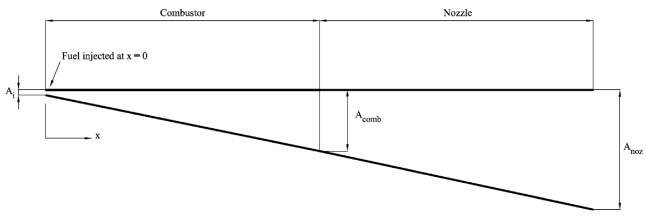

Fig. 5 Scramjet engine dimensions.

VI. Mission Profile

The mission involves launching a vehicle from Woomera, Australia that is capable of delivering a payload to a 200-km circular orbit. This requires an inertial velocity of 7784.3 m/s at an altitude of 200 km and a 0-deg flight path angle. Because this is an orbit with an inclination of −60 deg, the equivalent local horizontal velocity is 8202.9 m/s at the same conditions.

The first stage booster burns from the launch pad for 10 s to clear the dense lower altitude atmosphere. After a 45-s coast phase, the second booster stage ignites and accelerates the scramjet to an altitude of around 25 km, a Mach number of 7, and a 0-deg flight path angle.

For the hydrogen-fueled vehicle, the scramjet burns for approximately 345 s to achieve an altitude of 40 km, a local horizontal velocity of 4831 m/s (Mach 15), and a flight path angle of 1.4 deg. After scramjet shutdown, the angle of attack is set to 20 deg and the vehicle climbs to an altitude of 58.13 km, a local horizontal velocity of 4580 m/s, and a flight path angle of 0 deg. The upper stage is then released, which ignites once for injection at perigee into a 58.18 × 200 km low-Earth transfer orbit (LTO). After a coast to apogee, a second burn injects the payload into a 200-km circular orbit.

For the hydrocarbon-fueled vehicle (jet A), the scramjet burns for approximately 150 s to achieve an altitude of 33 km, a local horizontal velocity of 3096 m/s (Mach 10), and a flight path angle of 1.8 deg. After scramjet shutdown, the angle of attack is again set to 20 deg and the vehicle climbs to an altitude of 44.94 km, a local horizontal velocity of 2840 m/s, and a flight path angle of 0 deg. The upper stage is then released, which ignites once for injection at perigee into a 44.94 × 200 km LTO. After a coast to apogee, a second burn injects the payload into a 200-km circular orbit.

VII. Trajectory Profiles

Because of the different operating conditions of the two scramjets, their mission profiles will differ significantly. This section will show the mission profiles from the ignition of the first stage booster to the payload separation from the waverider. All conditions are shown in the local horizontal frame. It should be noted that the burn of the orbital stage is not shown.

A. Hydrogen-Fueled Waverider

Figure 6 shows the altitude profile for the vehicle with a hydrogen-fueled scramjet stage. At the beginning of the scramjet stage burn, the altitude is seen to have a shallower gradient compared with the end of the flight. This is because, in order to minimize the angle of attack

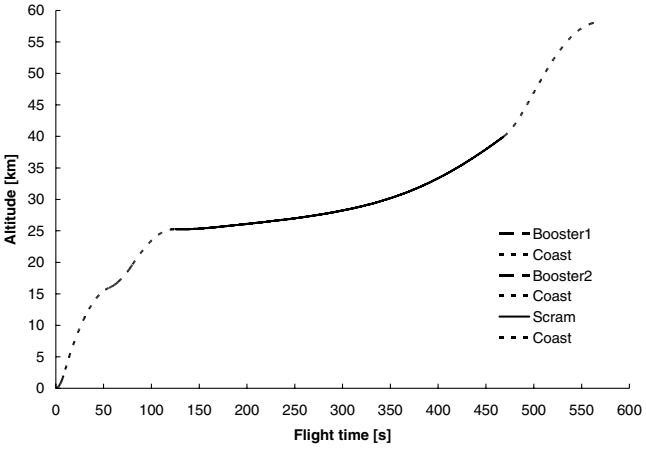

Fig. 6 Altitude profile for the hydrogen-fueled vehicle.

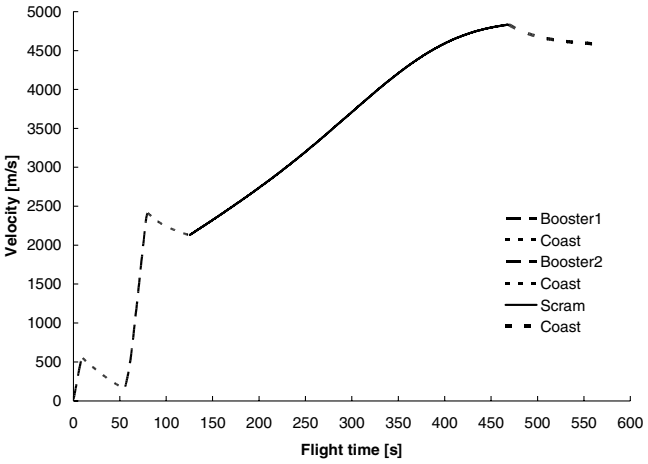

Fig. 7 Velocity profile for the hydrogen-fueled vehicle.

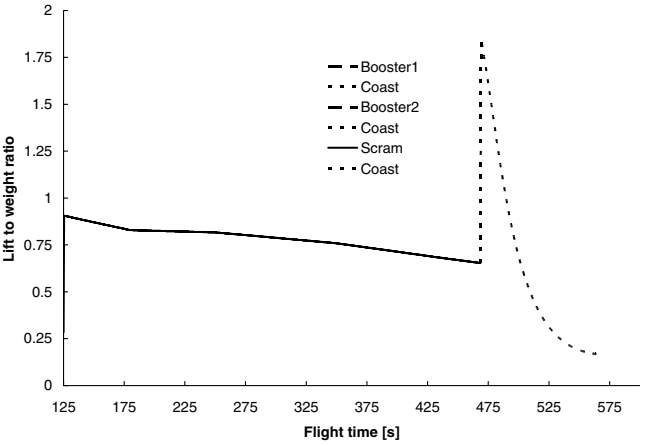

Fig. 9 Lift-to-weight ratio for the hydrogen-fueled vehicle.

while the vehicle is the heaviest and the slowest, a zero lift acceleration parameter was specified. Once the velocity had increased and the mass had decreased enough, a positive lifting acceleration could be used. Although the velocity is the highest and the mass the lowest at the end of the scramjet burn, the atmospheric density is also the lowest, thereby creating a low dynamic pressure regime in which a high angle of attack is required to achieve the required lifting acceleration.

Figure 7 shows the velocity profile for the hydrogen-fueled vehicle. A more linear profile is seen for most of the flight, with the velocity gradient only decreasing slightly at the end of the flight. This is because, at the beginning of the flight, the velocity is relatively low, but the atmospheric density is high. As the vehicle ascends, the atmospheric density decreases, whereas the velocity increases, thereby allowing a high thrust to be maintained. Only toward the end of the flight does the atmospheric density reduce significantly enough to reduce the thrust and cause the acceleration to decrease. The dynamic pressure during the scramjet burn ranged between 50 and 126 kPa.

As was mentioned in the Introduction, the angle of attack should be kept as low as possible, typically, not much above 5 deg. Figure 8 shows that during the scramjet burn, the angle of attack was kept below 6 deg. At scramjet shutdown, the angle of attack was set to 20 deg. This is seen by the increase in flight path angle and the drop in velocity at approximately 470-s flight time. This was done to achieve as high an altitude as possible at the ignition of the orbital stage, thereby minimizing the dynamic pressure on the payload. The stability of the vehicle at such a high angle of attack was found to be a problem in [6] and this issue would clearly need to be addressed in a control system analysis.

Figure 9 shows the lift-to-weight ratio for the scramjet-powered flight segment. It should be noted that the lift force is in the body coordinate system, whereas the weight is in the local horizontal frame. There is, therefore, a force component from the propulsion system that is also supporting part of the vehicle weight, hence the value below 1. This graph is not intended as a comparison between the two forces, but rather to illustrate the ratio between the aerodynamic lift force and the weight of the vehicle. It suggests that the propulsion system is used to increase the speed of the vehicle while at the same time supporting a portion of the weight of the vehicle. This is important, because it illustrates the fact that the aerodynamic reference area cannot be reduced significantly, because there is already no margin on the available lift force. Although there is no physical problem using the propulsion system to support the lift, the optimality of the vehicle design may be affected. A trade-off needs to be performed to determine if it is better to have a bigger, higher-drag engine to support the weight or whether to use a smaller engine with a larger lifting surface, also producing more drag. The actual trade-off is therefore a comparison between the extra drag contributions from the engine and the lifting surface. It may suggest that the vehicle size should be increased or, more likely, changed to increase the lift force; however, care must be taken, because an increase in lift area will also increase the drag force.

B. Hydrocarbon-Fueled Waverider

Figures 10 and 11 show the altitude and velocity profiles, respectively, for the hydrocarbon-fueled scramjet vehicle. Their behavior is similar to that seen for the hydrogen-fueled vehicle, except that the scramjet flight is noticeably shorter, due to the significantly reduced operating range. The dynamic pressure during the scramjet burn ranged between 58 and 114 kPa.

Figure 12 shows that in the case of the hydrocarbon-fueled scramjet, the angle of attack was also kept below 6 deg during the scramjet burn, with the angle of attack increasing 20 deg at the

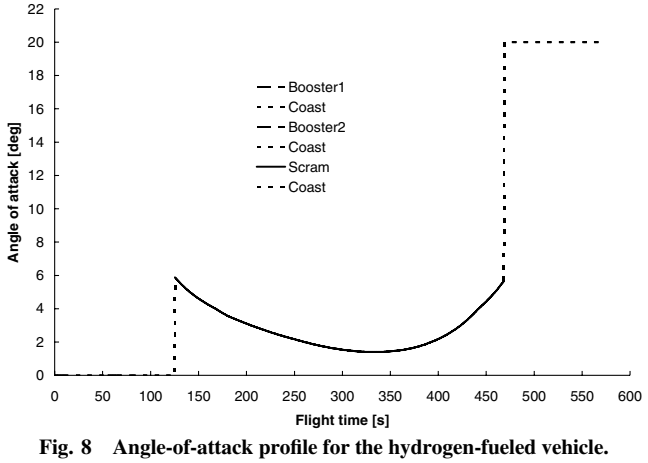

Fig. 8 Angle-of-attack profile for the hydrogen-fueled vehicle.

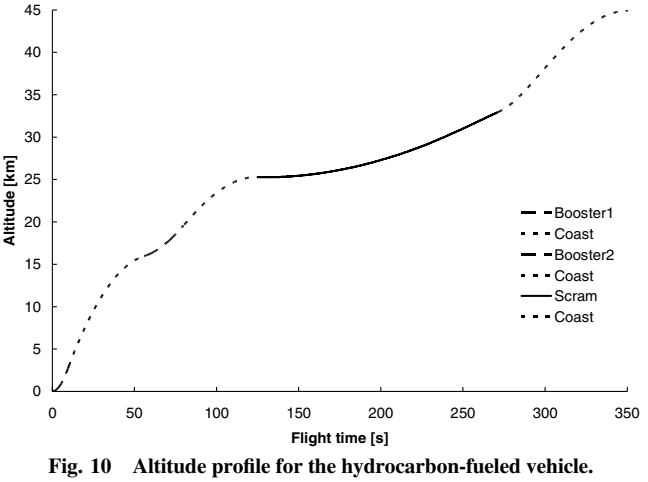

Fig. 10 Altitude profile for the hydrocarbon-fueled vehicle.

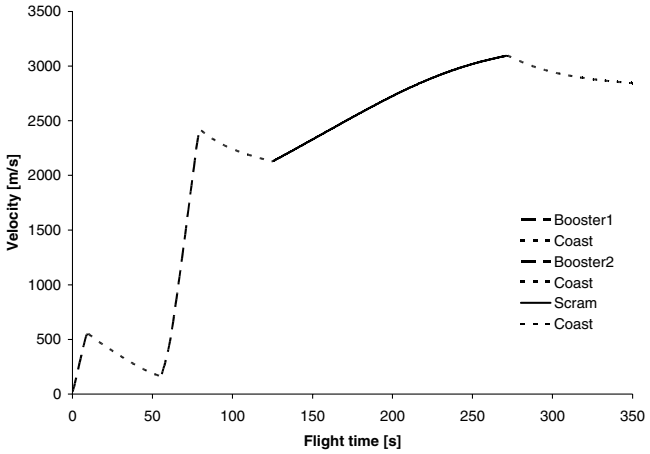

Fig. 11 Velocity profile for the hydrocarbon-fueled vehicle.

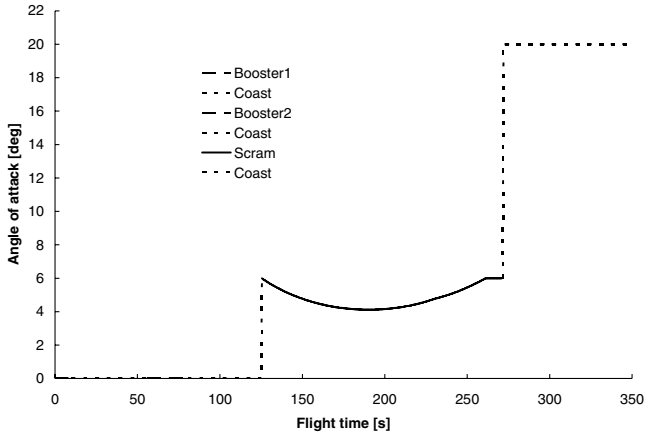

Fig. 12 Angle-of-attack profile for the hydrocarbon-fueled vehicle.

termination of the scramjet burn. The shape of the angle-of-attack profile is similar to that of the hydrogen-fueled vehicle, but again having a shorter operating period.

Figure 13 shows a similar result to Fig. 9 and is shown here for completeness. The reason for their similarity is that both vehicles had the same start mass and the same aerodynamic reference area.

C. Insertion Conditions

Table 3 shows the states at scramjet shutdown, which are the same as the start conditions for the upper stage, for which the mass included the dry waverider and the orbital stage. The launch system with the hydrogen-fueled scramjet stage achieves a significantly higher-energy transfer orbit than that for the hydrocarbon-fueled

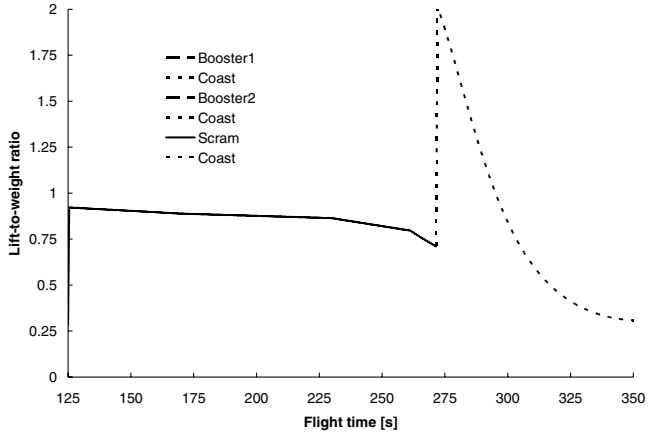

Fig. 13 Lift-to-weight ratio for the hydrocarbon-fueled vehicle.

Table 3 Conditions at orbital stage release

	Hydrogen-fueled vehicle	Hydrocarbon-fueled vehicle
Mass	1684 kg	1741 kg
Altitude	58.13 km	44.94
Velocity	4580 m/s	2840 m/s

system. The final mass for the hydrocarbon-fueled system is higher than that for the hydrogen-fueled system. Although more mass is available for the upper stage of the hydrocarbon-fueled system, the required energy input is even higher, making this system less favorable.

VIII. Mass and Volume Estimation

As was discussed in Sec. II, both the hydrogen and hydrocarbon-fueled waveriders had the same start mass of 2 t. From the point mass trajectory optimization, the fuel mass required for the scramjet burn could be calculated. Based on the fuel mass fraction of 0.58 and 0.7 [7] for hydrogen and hydrocarbon-fueled vehicles, respectively, the structure mass required for a scramjet without payload could be calculated using Eq. (8).

$$\varepsilon = m_{\text{fuel}}/m_{\text{total}} \tag{8}$$

Average payload density (based on launcher payload bay volumes and masses) varies considerably, depending on the launch vehicle. A representative payload mass-to-volume ratio (average density) is that of the Start-1 rocket, which is approximately 132 kg/m^3 [8]. Assuming an equivalent relationship exists between fuel and stage mass, and payload and stage mass, the structure required to house the scramjet payload can be estimated. A value of 0.6 was assumed for the payload mass to stage mass, based on the bounds of 0.58 for a 82 kg/m^3 substance (hydrogen) and 0.7 for an 800 kg/m^3 substance (jet A).

Hence, the waverider mass was estimated based on the fuel and the payload storage requirements. The scramjet dry mass is shown in Table 4. System mass comparison represents this combined mass. Note that the dry masses are different for the hydrogen and jet-A-powered vehicles, due to the better fuel storage density for the jet-A-fueled vehicles.

The remaining mass, after subtracting the scramjet dry mass and the fuel mass from the start mass, represents the mass available for the orbital stage. Considering the ΔV requirements to achieve orbit from the conditions stated in Table 3 and the performance measures of the orbital stage discussed in Sec. III.C, the payload masses for the two vehicles can be estimated.

The payload masses shown in Table 4 equate to a payload mass fraction of 1.24 and 0.39% for the hydrogen and hydrocarbon-powered vehicles, respectively.

Table 5 shows the volume budget for the two vehicles. From the upper stage mass and upper stage density, the volume required for the payload bay inside the waverider can be calculated. As discussed previously, the average upper stage density was taken to be 132 kg/m^3. The remaining waverider volume is then calculated by subtracting the total waverider volume and the fuel volume to determine if the upper stage can fit inside the waverider. It is unlikely that all of the remaining volume inside the waverider could be used to accommodate the upper stage, due to shape constraints; however, as

Table 4 System mass comparison

	Hydrogen-fueled scramjet	Hydrocarbon-fueled scramjet
Scramjet initial mass	2000 kg	2000 kg
Scramjet fuel mass	316 kg	258.8 kg
Scramjet dry mass	957 kg	926.2 kg
Upper stage mass	727 kg	815 kg
Payload mass	115.3 kg	36.0 kg

Table 5 Volume comparison

	Hydrogen-fueled scramjet	Hydrocarbon-fueled scramjet
Total waverider volume	16.229 m^3	16.229 m^3
Fuel volume	3.850 m^3	0.357 m^3
Remaining volume	12.275 m^3	15.772 m^3
Upper stage volume	5.5 m^3	6.17 m^3
Required fraction of remaining volume	44.8%	39.1%

Table 5 illustrates, less than half of the remaining volume would be required for the payload bay. Hence, these waveriders are expected to have sufficient volume capacity for the presented mission profiles.

IX. Discussion

The first observation is that the payload mass fraction for the launch systems with a hydrogen-powered scramjet stage is only slightly higher than those for fully rocket-powered launch systems. This is because, although the specific impulse for a scramjet-powered stage is considerably higher than that for a rocket stage, the fuel mass fraction is lower. Therefore, a similar total stage mass is required, but a larger portion of this mass is required for structure in the scramjet-powered case. This is due to the lower fuel storage efficiency of waveriders compared with rockets. Recall that a hydrogen-powered waverider has a fuel mass fraction of 0.58, whereas hydrocarbon-fueled waveriders can achieve 0.7. A rocket stage can have a fuel mass fraction of up to 0.94 [27].

This implies that, if the launch system is designed to be an expendable system, a scramjet stage would not be a financially viable option, because vehicle structure is much more expensive than propellant. If a scramjet-powered flight segment were to be considered in a launch system design, at least the scramjet stage would need to be reusable.

Although previous rocket-powered launch systems, such as the Space Shuttle, suggest that reusable launch systems are not financially beneficial [8], a scramjet-powered stage may be easier to make reusable, due to the few moving parts in the propulsion system. The scramjet stage proposed in this design is also suborbital and so would not need to endure an orbital reentry flight, again making reusability easier to achieve.

When comparing the hydrogen and jet-A-powered scramjet stages, it can clearly be seen that the hydrogen-powered vehicle has a significant payload advantage over the jet-A-powered vehicle. Although the jet-A-powered vehicle requires a lower dry mass to store its fuel, its Mach 10 operating limit and lower specific impulse override its dry mass advantage. The payload mass fraction of the launch system with a jet-A-powered waverider is seen to be below that of a fully conventional rocket-powered launch system.

Not only does the launch system with the hydrogen-powered waverider have an improved payload mass fraction, it also uses considerably less stored propellant during its ascent than that used by a fully rocket-powered system.

An observation made during the trajectory analysis was that the minimum dynamic pressure limit of 10 kPa for the scramjet operation was not reached. The minimum dynamic pressure required to lift the weight of the vehicle was higher than the engine operating limit at the end of flight. To overcome this absence of lift at high altitude, the lifting area of the scramjet could be increased. This would, however, increase the volume and mass of the vehicle.

The advantage of a jet-A-fueled waverider with an improved fuel storage density is not beneficial to the mission profile as the vehicle size and, therefore, volume cannot be reduced, due to the lift requirements.

The lift-to-weight profiles for the hydrogen-fueled and hydrocarbon-fueled vehicles are seen to be similar. This is due to the fact that the vehicle size is constant for both launch systems.

X. Conclusions

A similar payload mass fraction was found to be achievable using a launch system with a scramjet-powered stage and a fully rocket-powered system. Although less propellant was required for the scramjet-powered stage, the required structure mass was higher than that for a rocket-powered stage.

This implies that in order to make a launch system with a scramjet-powered stage economically feasible, at least the scramjet stage needs to be reusable. Scramjet-powered stages may be relatively easy to make reusable, due to there being few moving parts in the propulsion system. In addition, the scramjet-powered stage would not be required to perform an orbital reentry flight and, therefore, would not have stringent thermal protection system requirements.

For an orbital delivery launch system, a system with a hydrogen-powered scramjet stage was found to have a significantly higher payload capability than one with a jet-A-powered scramjet stage. This is due to the extended operating range of the hydrogen-fueled vehicle (up to Mach 15) and the higher specific impulse.

The advantage of improved fuel storage density for the jet-A-fueled case was found to not benefit an orbital mission. This is because insufficient lift is a limiting factor in achieving a desirable orbital stage release condition, and so the vehicle volume cannot be reduced, because this would reduce its lift capability.

The use of air-breathing propulsion for the Mach 0–7 flight would considerably enhance payload performance, especially for the jet A case. Similarly, the use of a scramjet/rocket stage in place of the orbital stage would also improve payload capability.

References

[1] Smart, M. K., Hass, N. E., and Paull, A. P., "Flight Data Analysis of the HyShot 2 Scramjet Flight Experiment," *AIAA Journal*, Vol. 44, No. 10, Oct. 2006, pp. 2366–2375.

[2] Moses, P. L., Rausch, V. L., Nguyen, L. T., and Hill, J. R., "NASA Hypersonic Flight Demonstrators: Overview, Status, and Future Plans," *Acta Astronautica*, Vol. 55, 2004, pp. 619–630.

[3] Fortescue, P., and Stark, J., *Spacecraft System Engineering*, Wiley, New York, 1995.

[4] Cohen-Zur, A., and Natan, B., "Experimental Investigation of a Supersonic Combustion Solid Fuel Ramjet," *Journal of Propulsion and Power*, Vol. 14, No. 6, 1998, pp. 880–889.

[5] Savino, R., and Pezzella, G., "Numerical Analysis of Supersonic Combustion Ramjet with Upstream Fuel Injection," *International Journal for Numerical Methods in Fluids*, Vol. 43, 2003, pp. 165–181.

[6] Curran, E. T., "Scramjet Engines: The First Forty Years," *Journal of Propulsion and Power*, Vol. 17, No. 6, Nov. Dec. 2001, pp. 1138–1148.

[7] Lewis, M. J., "Significance of Fuel Selection for Hypersonic Vehicle Range," *Journal of Propulsion and Power*, Vol. 17, No. 6, 2001, pp. 1214–1221.

[8] Isakowitz, S. J., *International Reference Guide to Space Launch Systems*, AIAA, Washington, D.C., 1995.

[9] Fry, R. S., "A Century of Ramjet Propulsion Technology Evolution," *Journal of Propulsion and Power*, Vol. 20, No. 1, Jan.–Feb. 2004, pp. 27–58.

[10] Grallert, H., and Keller, K., "Metallic Thermal Protection Concept for Hypersonic Vehicles," *Journal of Aircraft*, Vol. 28, No. 6, June 1991, pp. 410–416.

[11] Gaiddon, A., Knight, D. D., and Poloni, C., "Multicriteria Design Optimization of a Supersonic Inlet Based upon Global Missile Performance," *Journal of Propulsion and Power*, Vol. 20, No. 3, 2004, pp. 542–558.

[12] Cockrell, C. E., Huebner, L. D., and Finley, D. B., "Aerodynamic Characteristics of Two Waverider-Derived Hypersonic Cruise Configurations," NASA, Rept. 3559, 1996.

[13] Rahn, M., and Schoettle, U. M., "Decomposition Algorithm for Performance Optimization of a Launch Vehicle," *Journal of Spacecraft and Rockets*, Vol. 33, No. 2, 1996, pp. 214–221.

[14] Anderson, J. D., *Hypersonic and High Temperature Gas Dynamics*, AIAA, Reston, VA, 1989.

[15] Stuckey, R. M., and Lewis, M. J., "Hypersonic Missile Requirements and Operational Tradeoff Studies," *Journal of Spacecraft and Rockets*, Vol. 40, No. 2, 2003, pp. 292–293.

[16] Burkhardt, J., "REENT6D: a Simulation and Optimization Tool for Re-Entry Missions," Institut für Raumfahrtsysteme, Rept. IRS-01B7, Stuttgart, Germany, 2000.

[17] Regan, F. J., and Anandakrishnan, S. M., *Dynamics of Atmospheric Reentry*, AIAA Education Series, AIAA, Washington, D.C., 1993.
[18] Tetlow, M., "Commercial Launch Vehicle Design and Predictive Guidance Development," Ph.D. Dissertation, School of Mechanical Engineering, Univ. of Adelaide, Adelaide, Australia, 2003.
[19] O'Brien, T., Starkey, R., and Lewis, M., "Quasi-One-Dimensional High Speed Engine Model with Finite Rate Chemistry," *Journal of Propulsion and Power*, Vol. 17, No. 6, 2001, pp. 1366–1374.
[20] Hindmarsh, A. C., "ODEPACK, a Systemized Collection of ODE Solvers," *IMACS Transactions on Scientific Computation*, edited by R. S. Stepleman, North-Holland, Amsterdam, The Netherlands, 1983, pp. 55–64.
[21] Doolan, C. J., "A Supersonic Combustion Model for Scramjet Vehicle Performance Studies," *Proceedings of the 5th Asian-Pacific Conference on Combustion*, Combustion Inst., Pittsburgh, PA, 2005, pp. 457–460.
[22] Gerlinger, P., and Bruggeman, D., "Numerical Investigation of Hydrogen Strut Injectors into Supersonic Airflows," *Journal of Propulsion and Power*, Vol. 16, No. 1, 2000, pp. 22–28.
[23] Boyce, R. R., Paull, A., Stalker, R. J., Wendt, M., Chinzei, N., and Miyajima, H., "Comparison of Supersonic Combustion Between Impulse and Vitiation-Heated Facilities," *Journal of Propulsion and Power*, Vol. 16, No. 4, 2000, pp. 709–717.
[24] Kerrebrock, J. L., "Some Readily Quantifiable Aspects of Scramjet Engine Performance," *Journal of Propulsion and Power*, Vol. 8, No. 5, 1992, pp. 1116–1122.
[25] Heiser, W. H., and Pratt, D. T., *Hypersonic Airbreathing Propulsion*, AIAA, Reston, VA, 1994.
[26] Waltrup, P. J., "Upper Bounds on the Flight Speed of Hydrocarbon-Fueled Scramjet-Powered Vehicles," *Journal of Propulsion and Power*, Vol. 17, No. 6, Nov.–Dec. 2001, pp. 1199–1204.
[27] Huzel, D. K., and Huang, D. H., "Modern Engineering for the Design of Liquid-Propelled Rocket Engines," Vol. 47, Progress in Astronautics and Aeronautics, AIAA, Washington, D.C., 1992.

J. Martin
Associate Editor